Bulletin of the Seismological Society of America, Vol. 96, No. 6, pp. 2398–2414, December 2006, doi: 10.1785/0120060031

On the Accuracy of the Finite-Difference Schemes: The 1D Elastic Problem

by Jozef Kristek and Peter Moczo

Abstract We present a 1D finite-difference (FD) scheme that is based on the application of Geller and Takeuchi's (1998) optimally accurate FD operators to the heterogeneous strong-form equation of motion developed by Moczo *et al.* (2002). We numerically compare the scheme with two other FD schemes that approximate the heterogeneous strong-form equation of motion, one using conventional 2nd-order FD operators, the other using staggered-grid 4th-order FD operators. The numerical comparison is based on the envelope and phase misfits between tested and reference solutions. We discuss the error due to internal interface (primarily controlled by the boundary condition and its numerical approximation) and error due to grid dispersion. We demonstrate the superior accuracy of the scheme based on the application of the optimally accurate operators.

Introduction

Consider a 1D problem in a perfectly elastic isotropic medium with density ρ and Lamè's elastic coefficients μ and λ being continuous functions of z. Then a plane wave propagation in the z direction is described by the equation of motion and Hooke's law, in the displacement-stress (DS) formulation,

$$\rho \ddot{d} = \sigma_{,z} + f, \quad \sigma = C d_{,z}. \tag{1}$$

Here, $d(z,t)$ is the displacement, $\sigma(z,t)$ is stress, $f(z,t)$ is body force per unit volume either in the z direction, in the case of the P wave, or in a perpendicular direction, in the case of the S wave. Elastic modulus is $C(z) = \lambda(z) + 2\mu(z)$ in the first case or $C(z) = \mu(z)$ in the latter one. The double dot above the symbol means the time derivative. The subscript $,z$ in $\sigma_{,z}$ and $d_{,z}$ means the spatial derivative. Note that we could equivalently consider the displacement-velocity-stress or velocity-stress formulations instead of the displacement-stress formulation (e.g., Moczo *et al.*, 2004, 2006).

An alternative formulation is the so-called displacement (D) formulation

$$\rho \ddot{d} = (C d_{,z})_{,z} + f. \tag{2}$$

These formulations of the equation of motion are examples of strong formulations.

In principle, one can integrate the equation of motion over a spatial domain and then apply a FD approximation to the integrated equation (e.g., Sochacki *et al.*, 1991; Zahradník *et al.*, 1994). It is also possible to obtain a weak form of the equation of motion and apply the FD method to obtain its discrete approximation. Here we do not discuss this type of scheme.

Most of the FD schemes solve one of the strong forms in the time domain. Because only displacement values are explicitly present both in the displacement formulation of the equation of motion and conventional grid, since the early applications of the FD method in seismology, e.g., Alterman and Karal (1968), Boore (1970, 1972), the displacement FD schemes have been naturally formulated for the conventional grids. Because the conventional-grid displacement FD schemes had problems with instabilities in models with high-velocity contrasts and with grid dispersion in media with high Poisson's ratio, Virieux (1984, 1986) introduced the staggered-grid velocity-stress FD schemes for modeling seismic-wave propagation. To increase the computational efficiency, Levander (1988) introduced the 4th-order staggered-grid FD schemes. Then the staggered-grid FD schemes became the dominant type of schemes in the FD time-domain (FDTD) modeling of seismic-wave propagation and earthquake motion. For more see, for example, recent reviews of the FD modeling by Moczo *et al.* (2004, 2006).

The preceding displacement-stress formulation is also naturally connected with the staggered-grid schemes.

Among all FD schemes solving a strong-form equation of motion, the most popular are so-called heterogeneous FD schemes. This is because in a heterogeneous FD scheme all interior grid points (points not lying on borders of a grid) are treated in the same way no matter what their positions are with respect to the material discontinuity or smooth heterogeneity. The heterogeneity is accounted for only by assigning, say, effective grid values of elastic moduli and density to appropriate grid positions. The problem is that a strong-form equation solved by most of the heterogeneous FD schemes is not valid at a material discontinuity. If the strong-form equation is not valid at the material disconti-

nuity, its FD approximation can hardly be appropriate for media with material discontinuities.

Moczo *et al.* (2002) analyzed the 1D problem in a medium consisting of two half-spaces, that is, the problem of planar material discontinuity in a medium. They found such a form of the equation of motion and Hooke's law that is valid both at points outside a material discontinuity and at a point on the material discontinuity. We can call such a formulation a heterogeneous strong-form equation of motion. Moczo *et al.* (2002) also showed a simple physical model of the contact of two media.

The heterogeneous strong-form equation of motion can be, in principle, approximated by different FD schemes. In this study we compare three very different, and, at the same time, the most representative, approaches: applications of conventional, staggered-grid, and optimally accurate operators.

Geller and Takeuchi (1995, 1998) developed their optimally accurate FD schemes in application to the Galerkin-type weak form of Strang and Fix (1973) and Geller and Ohminato (1994). The clever idea of Geller and Takeuchi (1995) was to minimize the error of the numerical solution first at eigenfrequencies (or resonant frequencies), that is, at frequencies at which oscillatory motion of a linear mechanical system or finite volume of elastic continuum is naturally most amplified. Geller and Takeuchi (1995) derived a general criterion which requires that the inner product of an eigenfunction and the net error of the discretized equation of motion should be approximately equal to zero when the operand is the eigenfunction and the frequency is equal to the corresponding eigenfrequency. The criterion can be used to derive optimally accurate operators without knowing the actual values of the eigenfrequencies and eigenfunctions. Geller and Takeuchi (1995) showed that in a heterogeneous medium the criterion is the logical extension of the criterion to minimize grid dispersion of phase velocity for a homogeneous medium. Geller and Takeuchi (1998) used the criterion to develop optimally accurate 2nd-order FDTD scheme for the elastic 1D case. Takeuchi and Geller (2000) then developed optimally accurate FDTD operators for the 2D and 3D cases. Mizutani (2002) developed a scheme capable of accounting for an arbitrary position of the material discontinuity in the grid.

Other interesting approaches to minimize the error of a FD approximation include, for example, minimization of the relative error in group velocity caused by the grid dispersion within a specific frequency band emitted by active sources (Holberg, 1987) in the time domain, and schemes presented by Jo *et al.* (1996), Arntsen *et al.* (1998), and Štekl and Pratt (1998) in the frequency domain.

In this study we

- Apply the optimally accurate operators developed by Geller and Takeuchi (1998) to a heterogeneous strong formulation of the equation of motion developed by Moczo *et al.* (2002) for the 1D problem; we call the corresponding FD scheme Doptm2.
- Numerically compare Doptm2 with schemes based on application of standard conventional 2nd-order FD operators and staggered-grid 4th-order operators to a heterogeneous strong formulation of the equation of motion developed by Moczo *et al.* (2002) for the 1D problem; the two latter FD schemes are hereafter called Dconv2 and DSstag4, respectively.
- Numerically investigate error at the internal material discontinuity (we do not address the problem of the free surface) and error due to grid dispersion.

Note that we selected the three types of FD operators because they are the most representative among all developed and used FD operators. We restrict this study to the 1D problem because it is methodologically basic and important. Despite the relative simplicity of 1D problem, compared with the 3D problem, its numerical investigation yields extensive material, and, in our opinion, interesting and important findings. The 3D problem will by addressed by the authors in a separate study.

The Dconv2, DSstag4, and Doptm2 FD Schemes for a 1D Elastic Problem

The heterogeneous formulation of the 1D strong-form equation of motion is addressed in detail by Moczo *et al.* (2002); see also Moczo *et al.* (2004, 2006). We show here only equations that will be approximated by the three investigated FD schemes.

Displacement-Stress FD Scheme on the Staggered Grid: DSstag4

The equation of motion and Hooke's law for a point at the material discontinuity between two half-spaces (assumed for a while and without loss of generality at $z = 0$) have the form (Moczo *et al.*, 2002):

$$\bar{\rho}\,(0)\,\ddot{d}(0) = \overline{\sigma_{,z}}\,(0) + \bar{f}\,(0) \tag{3}$$

and

$$\sigma(0) = \overline{C}\,(0)\,\overline{d_{,z}}\,(0), \tag{4}$$

respectively, with a density equal to the arithmetic average of the densities in the two half-spaces, and elastic modulus equal to the harmonic average of the moduli in the two half-spaces:

$$\bar{\rho}\,(0) = 0.5 \cdot [\rho^{-}(0) + \rho^{+}(0)], \tag{5}$$

and

$$\overline{C}\,(0) = 2/[1/C^{-}(0) + 1/C^{+}(0)]. \tag{6}$$

The average spatial derivatives of the stress and displacement are

$$\overline{\sigma_{,z}}(0) + \bar{f}(0) = 0.5 \cdot [\sigma_{,z}^{-}(0) + \sigma_{,z}^{+}(0) + f^{-}(0) + f^{+}(0)]$$
$$\overline{d_{,z}}(0) = 0.5 \cdot [d_{,z}^{-}(0) + d_{,z}^{+}(0)]. \quad (7)$$

Equations (3) and (4) for a point at the material discontinuity have the same form as the equation of motion and Hooke's law at a point away from the material discontinuity.

If we neglect averaging of the spatial derivatives at the interface, a simple FD approximation to the preceding heterogeneous displacement-stress formulation of the equation of motion can be written as

$$T^m_{I+1/2} = C^H_{I+1/2}\frac{1}{h}\left[a(D^m_{I+2} - D^m_{I-1}) + b(D^m_{I+1} - D^m_I)\right]$$
$$D^{m+1}_I = 2D^m_I - D^{m-1}_I + \frac{1}{\rho^A_I}\frac{\Delta^2 t}{h}\left[a(T^m_{I+3/2} - T^m_{I-3/2}) + b(T^m_{I+1/2} - T^m_{I-1/2})\right] + \frac{\Delta^2 t}{\rho^A_I}F^m_I \quad (8)$$

where $T^m_{I+1/2}$, D^m_I, and F^m_I are discrete approximations to stress, displacement, and body-force values σ ($[I + 1/2]h$, $m\,\Delta t$), d ($I\,h$, $m\,\Delta t$), and f ($I\,h$, $m\,\Delta t$), respectively, $a = -1/24$, $b = 9/8$, Δt is the timestep, h is spatial grid spacing, and ρ^A_I and $C^H_{I+1/2}$ are given by (Moczo *et al.*, 2002)

$$\rho^A_I = \frac{1}{h}\int_{z_{I-1/2}}^{z_{I+1/2}} \rho(z)\,dz, \quad (9)$$

$$C^H_{I+1/2} = \left[\frac{1}{h}\int_{z_I}^{z_{I+1}} \frac{1}{C(z)}\,dz\right]^{-1}. \quad (10)$$

In the scheme, referred to hereafter as DSstag4, the spatial operator is fourth-order accurate, time operator second-order accurate. A computer algorithm performing schemes (8) can be designed to involve four multiplications and nine additions.

Displacement FD Schemes on the Conventional Grid: Dconv2 and Doptm2

The equation of motion for a point at the material discontinuity between two half-spaces (also here assumed at $z = 0$) has the form

$$\bar{\rho}(0)\,\ddot{\bar{d}}(0) = \overline{(Cd_{,z})_{,z}}\Big|_{z=0} + \bar{f}(0). \quad (11)$$

Here, the average density $\bar{\rho}(0)$ and body force $\bar{f}(0)$ are given by equations (5) and (7), respectively, and

$$\overline{(Cd_{,z})_{,z}}|_{z=0} = \frac{1}{2}\left[(Cd_{,z})^{-}_{,z}\Big|_{z=0} + (Cd_{,z})^{+}_{,z}\Big|_{z=0}\right]. \quad (12)$$

In a simple FD approximation we neglect the averaging of derivatives at the interface. Thus we approximate single term $(Cd_{,z})_{,z}$ using the 2nd-order central difference

$$(Cd_{,z})_{,z}\,|_I \doteq \frac{1}{h}\left(Cd_{,z}\Big|_{I+1/2} - Cd_{,z}\Big|_{I-1/2}\right). \quad (13)$$

Then, we approximate $Cd_{,z}$ in the same way as we approximated stress in the DS formulation.

To be concise, we approximately follow notation used by Geller and Takeuchi (1995, 1998) to formulate the scheme based on the application of the 2nd-order conventional operator, Dconv2, and the scheme based on the application of the 2nd-order optimally accurate operators, Doptm2. A FD approximation to equation (11) can be written as

$$\left[A^m_I(M,i) - K^m_I(M,i)\right]D(M,i) = F^m_I, \quad (14)$$

where m is the time level, at which the equation of motion is approximated, I is the index of the grid spatial position at which the equation of motion is approximated, M is the time summation index, and i is the spatial summation index. Matrices $\mathbf{A}^m_I$ and $\mathbf{K}^m_I$ are

$$\mathbf{A}^m_I(M,i) = \begin{bmatrix} a^{m+1}_{I-1}\rho_{I-1} & a^{m+1}_I\rho_I & a^{m+1}_{I+1}\rho_{I+1} \\ a^m_{I-1}\rho_{I-1} & a^m_I\rho_I & a^m_{I+1}\rho_{I+1} \\ a^{m-1}_{I-1}\rho_{I-1} & a^{m-1}_I\rho_I & a^{m-1}_{I+1}\rho_{I+1} \end{bmatrix} \quad (15)$$

and

$$\mathbf{K}^m_I(M,i) = \begin{bmatrix} k^{m+1}_{I-1}C_{I-1} & k^{m+1}_I C_I & k^{m+1}_{I+1}C_{I+1} \\ k^m_{I-1}C_{I-1} & k^m_I C_I & k^m_{I+1}C_{I+1} \\ k^{m-1}_{I-1}C_{I-1} & k^{m-1}_I C_I & k^{m-1}_{I+1}C_{I+1} \end{bmatrix}. \quad (16)$$

For Dconv2, the matrices are

$$\mathbf{A}^m_I = \frac{\rho^A_I}{\Delta^2 t}\begin{bmatrix} 0 & 1 & 0 \\ 0 & -2 & 0 \\ 0 & 1 & 0 \end{bmatrix} \quad (17)$$

and

$$\mathbf{K}_I^m = \frac{1}{h^2}\begin{bmatrix} 0 & 0 & 0 \\ 1 & -2 & 1 \\ 0 & 0 & 0 \end{bmatrix} \begin{bmatrix} C^H_{I-1/2} & & 0 & 0 \\ 0 & \frac{1}{2}(C^H_{I-1/2} + C^H_{I+1/2}) & 0 & \\ 0 & & 0 & C^H_{I+1/2} \end{bmatrix}. \tag{18}$$

For Doptm2, the matrices are

$$\mathbf{A}_I^m = \frac{\rho_I^A}{\Delta^2 t}\begin{bmatrix} 1/12 & 10/12 & 1/12 \\ -2/12 & -20/12 & -2/12 \\ 1/12 & 10/12 & 1/12 \end{bmatrix} \tag{19}$$

and

$$\mathbf{K}_I^m = \frac{1}{h^2}\begin{bmatrix} 1/12 & -2/12 & 1/12 \\ 10/12 & -20/12 & 10/12 \\ 1/12 & -2/12 & 1/12 \end{bmatrix} \begin{bmatrix} C^H_{I-1/2} & & 0 & 0 \\ 0 & \frac{1}{2}(C^H_{I-1/2} + C^H_{I+1/2}) & 0 & \\ 0 & & 0 & C^H_{I+1/2} \end{bmatrix}. \tag{20}$$

Both Dconv2 and Doptm2 are formally 2nd-order accurate in space and time. In the case of a homogeneous medium the matrices take simpler forms:

$$\mathbf{A}_I^m = \frac{\rho}{\Delta^2 t}\begin{bmatrix} 0 & 1 & 0 \\ 0 & -2 & 0 \\ 0 & 1 & 0 \end{bmatrix}, \qquad \mathbf{K}_I^m = \frac{C}{h^2}\begin{bmatrix} 0 & 0 & 0 \\ 1 & -2 & 1 \\ 0 & 0 & 0 \end{bmatrix} \tag{21}$$

for Dconv2 and

$$\mathbf{A}_I^m = \frac{\rho}{\Delta^2 t}\begin{bmatrix} 1/12 & 10/12 & 1/12 \\ -2/12 & -20/12 & -2/12 \\ 1/12 & 10/12 & 1/12 \end{bmatrix}, \qquad \mathbf{K}_I^m = \frac{C}{h^2}\begin{bmatrix} 1/12 & -2/12 & 1/12 \\ 10/12 & -20/12 & 10/12 \\ 1/12 & -2/12 & 1/12 \end{bmatrix} \tag{22}$$

for Doptm2.

Note that in the 1D case, Dconv2 is equivalent to DSstag2, which is the 2nd-order displacement-stress staggered-grid FD scheme.

Whereas Dconv2 and DSstag2 are explicit FD schemes, it is clear from equations (19) and (20) that Doptm2 is an implicit scheme. We solve the implicit scheme by the predictor-corrector algorithm as suggested by Geller and Takeuchi (1998). A computer algorithm performing Dconv2 can be designed to involve three multiplications and three additions or two multiplications and six additions. The two cases have different memory requirements. The algorithm for Doptm2 involves six multiplications and nine additions. The same numbers were found by Geller and Takeuchi (1998); their 1D optimally accurate scheme and Doptm2 have, obviously, the same structure.

Analytical Solution

Consider a homogeneous half-space with index 1 separated from a homogeneous half-space with index $n + 1$ by a stack of $n - 1$ homogeneous layers with indices 2, 3, . . ., n. A thickness of the jth layer is h_j, velocity and density in the jth layer are c_j and ρ_j. Let a coordinate axis z be oriented positive in the direction of increasing layer index. Let interface between half-space 1 and layer 2 be at $z_1 = 0$ and interface between layers $j - 1$ and j, say, the upper boundary of layer j, at $z_{j-1} = \sum_{k=2}^{j-1} h_k$; see Figure 1. Assume a known wave propagating in the negative z direction from half-space $n + 1$ through the stack of layers into half-space 1. Then displacement in half-space 1 is

$$d^{(1)}(z,t) = F^{-1}\{S(f) \cdot H^{(1)}(z,f)\}; \quad z \le 0. \tag{23}$$

Here F^{-1} is the inverse Fourier transform, $S(f)$ is the spectrum of an input signal (spectrum of a source time function), and $H^{(1)}(f)$ is the transfer function

$$H^{(1)}(z,f) = \frac{2\omega q_{n+1}}{\omega(q_1 A_{22} + q_{n+1} A_{11}) + i(A_{21} - \omega^2 q_1 q_{n+1} A_{12})} \exp\left(\frac{-i2\pi f z}{c_1}\right) \tag{24}$$

with angular frequency $\omega = 2\pi f$, wave impedance $q_j = \rho_j c_j$, matrix $\mathbf{A} = \mathbf{A}_n \mathbf{A}_{n-1} \ldots \mathbf{A}_2$, layer matrix

$$\mathbf{A}_j = \begin{bmatrix} \cos b_j & \frac{\sin b_j}{\omega q_j} \\ -\omega q_j \sin b_j & \cos b_j \end{bmatrix}, \tag{25}$$

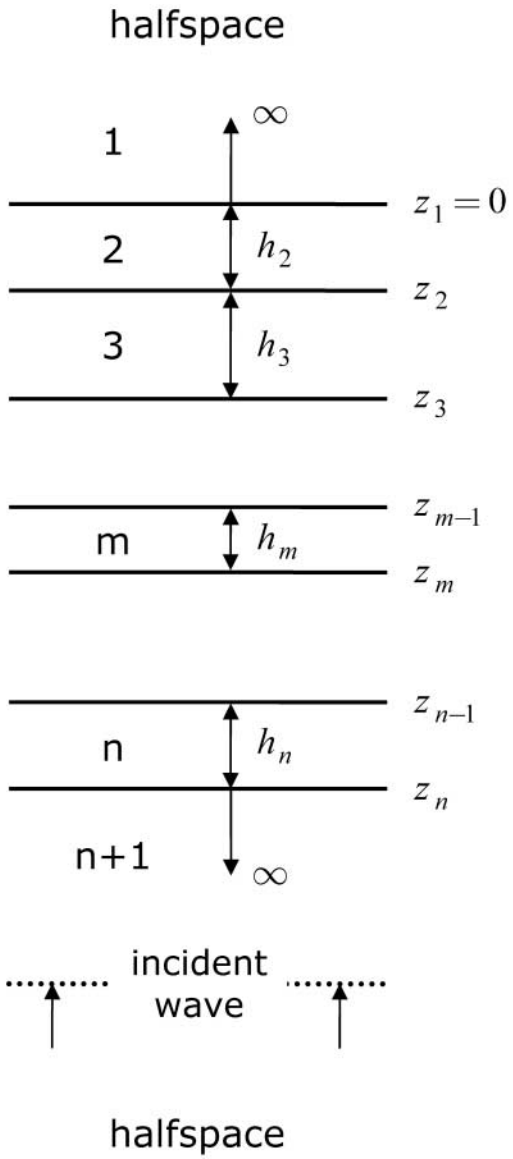

Figure 1. A 1D model of a stack of horizontal parallel homogeneous elastic layers between two half-spaces. The ith layer is characterized by velocity c_i, density ρ_i, and thickness h_i. The half-spaces are characterized by velocities c_1 and c_{n+1}, and densities ρ_1 and ρ_{n+1}, respectively.

and $b_j = \omega h_j/c_j$. In the limit case of a contact of two half-spaces we have simple

$$H^{(1)}(z, f) = \frac{2q_2}{q_1 + q_2} \exp\left(\frac{-i2\pi f z}{c_1}\right). \quad (26)$$

The displacement in layer j is

$$d^{(j)}(z,t) = F^{-1}\left\{S(f) \cdot H^{(j)}(z, f)\right\}; \quad z_{j-1} \le z \le z_j; \quad 2 \le j \le n. \quad (27)$$

Here,

$$H^{(j)}(z, f) = \left\{B^+ \exp\left[\frac{i\omega}{c_j}(z - z_{m-1})\right] - B^- \exp\left[-\frac{i\omega}{c_j}(z - z_{m-1})\right]\right\} \frac{2\omega q_{n+1}}{B^+D^- - B^- D^+} \quad (28)$$

with

$$B^\pm = A_{21}^{(U)} \pm \omega^2 q_1 q_j A_{12}^{(U)} - i\omega\left(q_1 A_{22}^{(U)} \mp q_j A_{11}^{(U)}\right)$$
$$D^\pm = \omega\left(q_{n+1} A_{11}^{(L)} \pm q_j A_{22}^{(L)}\right) + i\left(A_{21}^{(L)} \mp \omega^2 q_j q_{n+1} A_{12}^{(L)}\right) \quad (29)$$

and

$$\mathbf{A}^{(L)} = \mathbf{A}_n A_{n-1} \cdots A_j, \quad \mathbf{A}^{(U)} = \mathbf{A}_{j-1}\mathbf{A}_j \cdots \mathbf{A}_2. \quad (30)$$

The preceding formulas were used to calculate reference (exact) solutions for the models of two half-spaces and stack of layers.

Envelope and Phase Misfits

Consider a signal $s(t)$ that is to be compared with a reference signal $s_{\text{ref}}(t)$. Let $\hat{s}(t)$ and $\hat{s}_{\text{ref}}(t)$ be analytical signals corresponding to $s(t)$ and $s_{\text{ref}}(t)$, respectively. Simple estimates of the envelope and phase misfits of signal $s(t)$ with respect to $s_{\text{ref}}(t)$ can be defined as (Kristek *et al.*, 2002)

$$EM = \sqrt{\sum_t \left(|\hat{s}(t)| - |\hat{s}_{\text{ref}}(t)|\right)^2} \Big/ \sqrt{\sum_t |\hat{s}_{\text{ref}}(t)|^2} \quad (31)$$

and

$$PM = \frac{\sqrt{\sum_t \left(|\hat{s}_{\text{ref}}(t)| \frac{\{\text{Arg}[\hat{s}(t)] - \text{Arg}[\hat{s}_{\text{ref}}(t)]\}}{\pi}\right)^2}}{\sqrt{\sum_t |\hat{s}_{\text{ref}}(t)|^2}}. \quad (32)$$

These misfits give practically the same numerical values as those defined by Kristekova *et al.* (2006) if the signals are as simple as in this study.

Wave-Field Excitation in the FD Simulations

Wave is radiated from a chosen grid point in a chosen direction by using the Alterman and Karal (1968) decomposition in which a displacement corresponding to a source time function is prescribed. The source time function used in numerical simulations is Gabor signal, that is, a harmonic carrier with a Gaussian envelope, $s(t) = \exp\{-[\omega_p(t - t_s)/\gamma_s]^2\} \cos[\omega_p(t - t_s) + \theta]$. Here, $\omega_p = 2\pi f_p$, $t \in \langle 0, 2t_s \rangle$,

$f_p = 0.5$ Hz is predominant frequency, $\gamma_s = 11$ controls the width of the signal, $\theta = \pi/2$ is a phase shift, and $t_s = 0.45\gamma_s/f_p$. The amplitude spectrum of the signal is shown in Figure 2. The amplitude spectrum falls from its maximum at the frequency $f_{\mathrm{DOM}} = 0.5$ Hz by three orders of magnitude down to a value at $f_{\mathrm{MAX}} = 0.74$ Hz. In other words, the signal has relatively narrow spectrum with a dominant frequency.

In the implementation of the Alterman-Karal (1968) decomposition, the wave field is radiated in a lower half-space at a distance of $13h/2$ from the interface (see Fig. 6). To match this distance of radiation in the analytical calculation, a formal layer (the same material as in the lower half-space) with thickness of $13h/2$ was considered in the lower half-space.

Homogeneous Space

Consider a homogeneous perfectly elastic medium with wave velocity $c = 3464$ m/sec and density $\rho = 2700$ kg/m^3. Define

$$\lambda_{\mathrm{DOM}} = c/f_{\mathrm{DOM}} = c/0.5 \text{ m} \quad \text{and} \qquad \lambda_{\mathrm{MIN}} = c/f_{\mathrm{MAX}} = c/0.74 \text{ m}. \tag{33}$$

Let h be a grid spacing, N is the number of grid spacings per λ_{MIN}, that is,

$$N = \lambda_{\mathrm{MIN}}/h. \tag{34}$$

As shown by Geller and Takeuchi (1998), the conventional and optimally accurate operators satisfy the same stability condition (the Courant stability condition)

$$\Delta t \le \frac{h}{c}. \tag{35}$$

The stability condition for the 4th-order staggered-grid scheme is, for example, Moczo *et al.* (2004),

$$\Delta t \le \frac{6}{7}\frac{h}{c}. \tag{36}$$

Then the corresponding stability ratios are

$$p = \frac{c}{h}\Delta t \tag{37}$$

and

$$p = \frac{7c}{6h}\Delta t, \tag{38}$$

respectively. In any case, $p \le 1$, that is, p is a fraction of the maximum possible timestep.

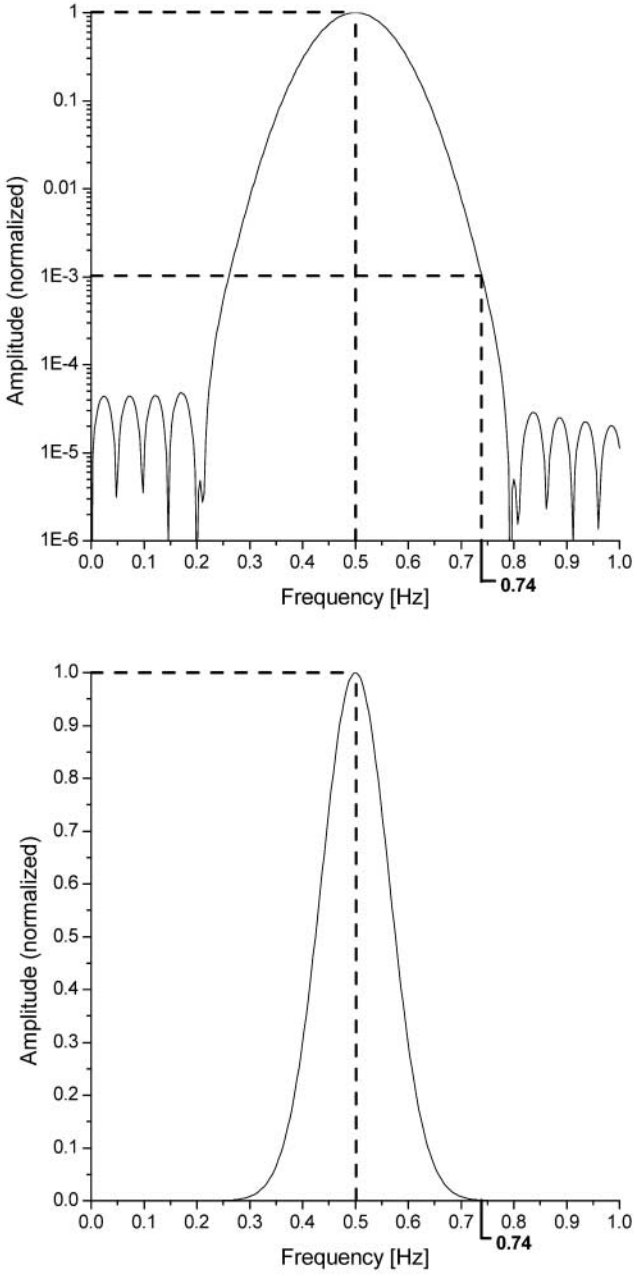

Figure 2. Amplitude Fourier spectrum of Gabor signal used as the source time function in numerical tests.

Figure 3 shows envelope and phase misfits of the FD schemes Dconv2, DSstag4, and Doptm2 as functions of N and $p \in \{0.10, 0.15, \ldots, 0.95\}$ at three propagation distances, λ_{DOM}, $10\lambda_{\mathrm{DOM}}$, and $20\lambda_{\mathrm{DOM}}$, from the grid point at which the wave is radiated. Whereas the misfits of Dconv2 and Doptm2 are shown for $N \in \{10, 11, \ldots, 30\}$, the misfits for DSstag4 are shown for $N \in \{5, 6, \ldots, 30\}$. This is because many users of the 4th-order staggered-grid schemes use N as low as 5 or 6. Based on Figure 3 we can summarize the following.

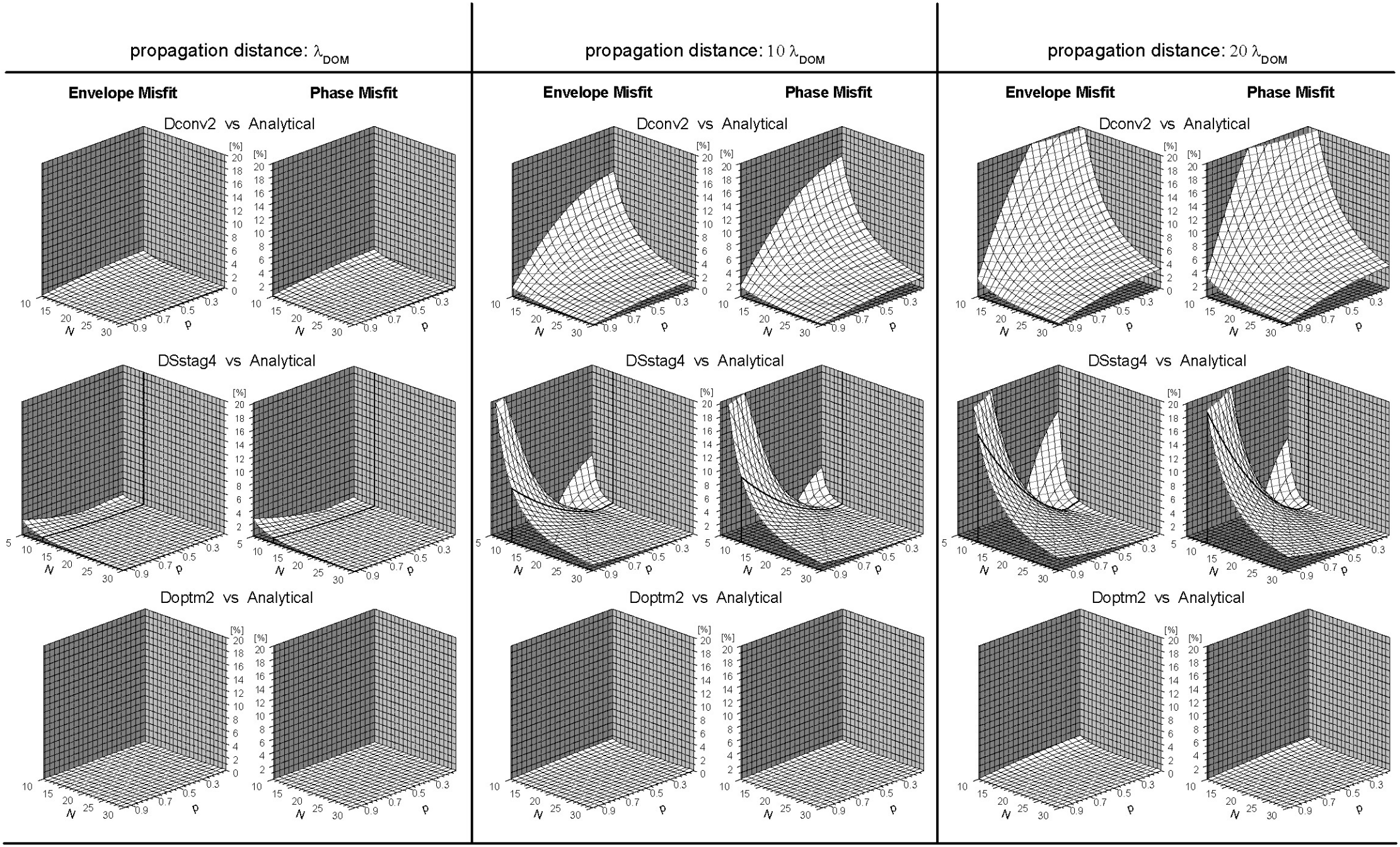

Figure 3. Error of propagation in a homogeneous space: envelope and phase misfits of the FD schemes Dconv2, DSstag4, and Doptm2 as functions of N (the number of grid spacings per λ_{MIN}) and ρ (the stability ratio) at three propagation distances (λ_{DOM}, $10\lambda_{DOM}$, and $20\lambda_{DOM}$) from the grid point at which the wave is radiated. The misfits are evaluated relative to the reference analytical solution.

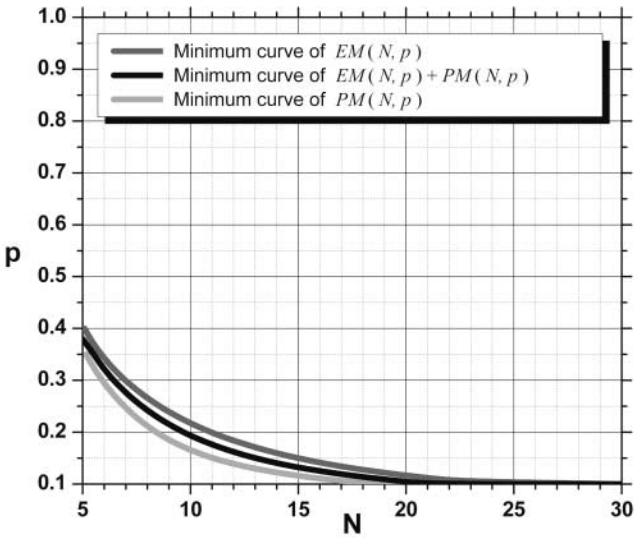

Figure 4. Curves of minima of the envelope misfit *EM*(*N*,*p*), phase misfit *PM*(*N*,*p*), and sum of the two misfits *EM*(*N*,*p*) + *PM*(*N*,*p*) as functions of *N* and *p*.

Dconv2 (Equivalent to DSstag2). For given *N* and distance the error monotonically grows with decreasing *p*. For given *p* and distance the error monotonically decreases with *N*. For given *N* and *p* the error monotonically grows with distance. The growth of the error is significant. Note that at the limit case of $p = 1$ the scheme is accurate. This is because the grid phase velocity is accurate in such a case (e.g., Geller and Takeuchi, 1998).

Dstag4. For a given distance, the error as a function of *p* is not monotonic for *N* smaller than some value: it decreases from its maximum for $p = 1$ down to some minimum and then increases again with decreasing *p*. For small *N* and large *p* the error is considerably larger than that of Dconv2. For given *N* and *p* the error monotonically grows with distance.

An implication for numerical calculations using Dstag4 is that in the homogeneous medium an adjusted, sufficiently small *p* has to be used for a chosen *N* to reduce grid dispersion. Figure 4 shows curves of minima of the envelope misfit, phase misfit, and sum of the two misfits as functions of *N* and *p*, that is, *EM*(*N, p*), *PM*(*N, p*), and *EM*(*N, p*) + *PM*(*N, p*). The curves were constructed from the numerical calculations for the propagation distance of $20\lambda_{\mathrm{DOM}}$ shown in Figure 3. In a homogeneous medium, for a chosen *N*, such *p* should be taken, for which *EM*(*N, p*) + *PM*(*N, p*) takes the minimum value. *EM*(*N, p*) along its minimum curve as well as *PM*(*N, p*) along its minimum curve should theoretically be equal to zero because they correspond to (*N, p*) curve with zero grid dispersion. Because the errors were determined numerically, they are not strictly zero.

Doptm2. Compared with the Dconv2 and DSstag4, the error is negligible; its relatively slow growth with distance can be seen (in Fig. 3) only for unreasonably small *N*.

Figure 5 compares the envelope and phase misfits at wave-propagation distances of $10\lambda_{\mathrm{DOM}}$ and $20\lambda_{\mathrm{DOM}}$ for two values of the stability ratio $p \in \{0.20, 0.95\}$. The misfit values smaller than $1\mathrm{E}-3$ are not shown because the numerical calculations are not accurate enough to properly evaluate smaller misfits. The phase misfit for Dconv2 at a distance of 20λ, and for $N < 6$, is larger than 1 (which means phase shift by π); therefore, it is not shown in the figure.

For $p = 0.95$, that is close to the maximum possible timestep, DSstag4 is the least accurate, even less accurate than the 2nd-order Dconv2 scheme. The rates of convergence of DSstag4 and Dconv2 are the same: the slope of the lines is -2. This is an important aspect because DSstag4 formally is the 4th-order, whereas Dconv2 is only 2nd-order accurate. Doptm2 clearly is the more accurate with the rate of convergence equal to -4. The convergence rates are the same for both the envelope and phase misfits.

For $p = 0.20$ the picture looks very different because of the previously mentioned fact that the error of DSstag4 as a function of *p* is not monotonic for *N* smaller than some value. The low values of the envelope and phase errors are because the DSstag4 phase velocity in homogeneous medium is exact for some low values of *p* and *N* as shown by R. J. Geller *et al.* (unpublished work) and N. Hirabayashi *et al.* (unpublished work).

Note that although such an adjustment of the stability ratio *p* value is possible with DSstag4 in the homogeneous medium (at a price of a small fraction of the maximum possible timestep), it is not possible in general in the heterogeneous medium. Therefore, the small errors of the DSstag4 shown in Figure 5 do not mean that DSstag4 could compete in accuracy with Doptm2 in heterogeneous models.

Two Half-Spaces Separated by a Planar Interface

Let c_1 be velocity in the half-space, where the plane wave is radiated, c_2 velocity in the half-space, where the transmitted wave is observed, and $c_1 > c_2$. In the numerical simulations $c_1 = 3464$ m/sec and $c_2 \in \{2310.0, 1819.1, 1328.2, 837.3, 346.4\}$ m/sec were used. The corresponding velocity contrasts are $c_1/c_2 \in \{1.5, 1.9, 2.6, 4.1, 10.0\}$. Densities were $\rho_1 = 2700$ kg/m^3 and $\rho_2 = 2500$ kg/m^3.

The interface is located midway between two grid points (see Fig. 6). Note that such a position of the interface is not necessary; the interface could be placed anywhere. We chose the interface position in-between two grid points (i.e., not at a grid point) to demonstrate the capability of the heterogeneous schemes based on the approach by Moczo *et al.* (2002) to sense the position of the interface in the grid.

In all three schemes the wave is radiated in the half-space with c_1 at a distance of 6.5 grid spacings from the interface that is the minimum distance in the Alterman-Karal radiation (1968) applied in the 4th-order staggered-grid scheme.

In principle we could consider a timestep in each of the two half-spaces,

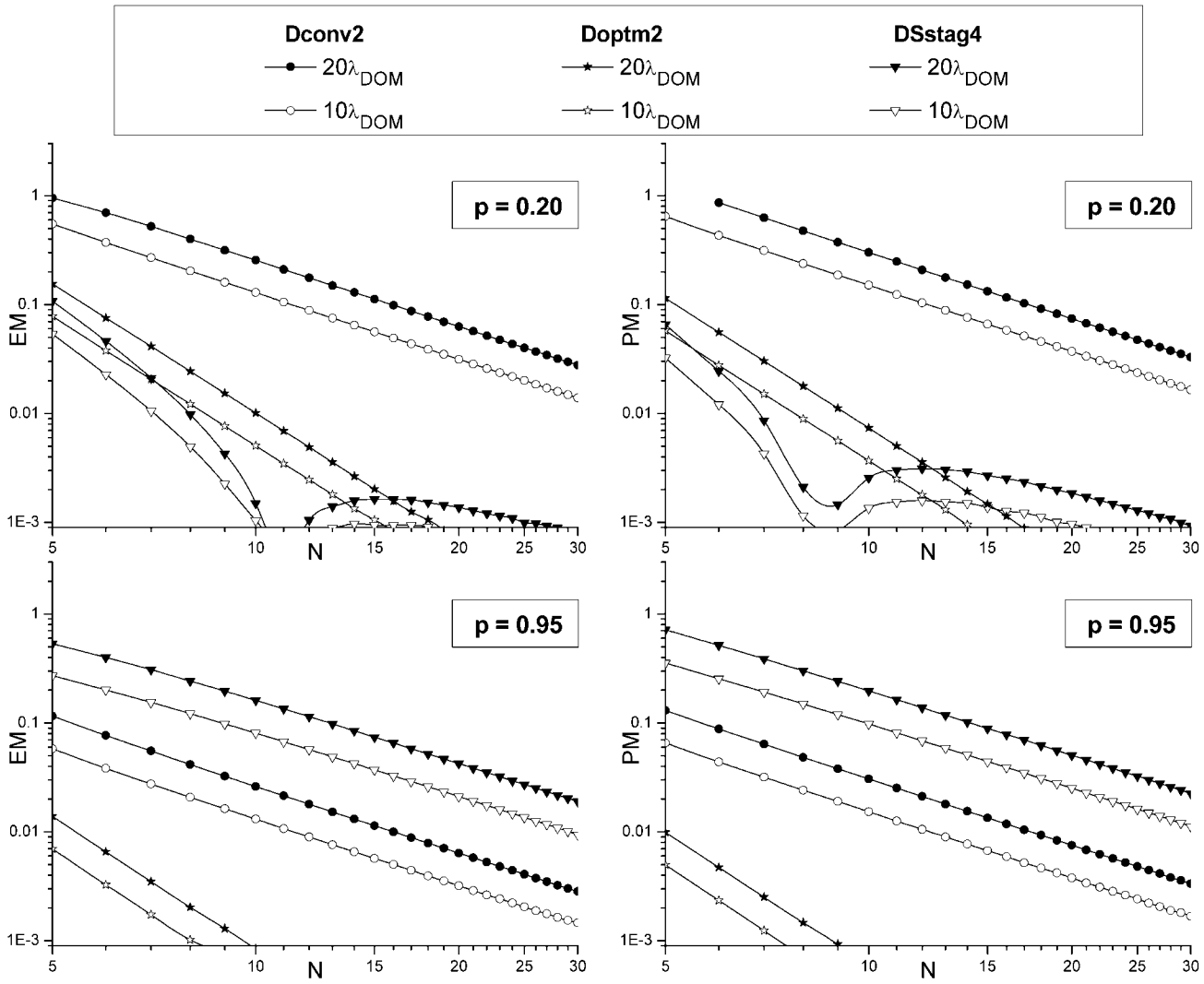

Figure 5. The envelope and phase misfits, *EM* and *PM*, as functions of N shown for $p \in \{0.20, 0.95\}$ at two travel distances of $10\lambda_{\mathrm{DOM}}$ and $20\lambda_{\mathrm{DOM}}$.

$$\Delta t_i = p_i \gamma \frac{h_i}{c_i}; \quad i = \{1,2\}, \tag{39}$$

with γ, coefficient corresponding to a particular FD scheme, and p_i, stability ratio (fraction of the timestep). If the same spatial grid spacing,

$$h = \frac{\lambda_{\mathrm{MIN}} c_2}{N} = \frac{c_2}{N \cdot f_{\mathrm{MAX}}}, \tag{40}$$

is used in the whole model, then

$$\Delta t_1 = p_1 \gamma \frac{1}{N \cdot f_{\mathrm{MAX}}} \frac{c_2}{c_1}, \quad \Delta t_2 = p_2 \gamma \frac{1}{N \cdot f_{\mathrm{MAX}}}. \tag{41}$$

If the same timestep, obviously determined by c_1 ($>c_2$), is used in the whole model, then

$$\frac{1}{p_2} = \frac{1}{p_1} \frac{c_1}{c_2}, \tag{42}$$

which means that for a fixed p_1, fraction p_2 of the timestep in the c_2-half-space decreases with velocity contrast c_1/c_2.

Receivers were located in the c_2-half-space. The first receiver was at a grid point located half-grid spacing from the interface. Other receivers were at distances $\{1,2,\ldots,20\} \times \lambda_{\mathrm{DOM}}\,(c_2)$ from the first receiver.

Figure 7 shows envelope and phase misfits for three of the five calculated velocity contrasts: 1.5, 4.1, and 10.0. In the numerical calculations $p_1 = 0.95$ was used. The observations can be summarized as follows.

Error at the Interface

For a given N the envelope misfit of each scheme at the interface weakly grows with c_1/c_2. The phase misfit is considerably smaller in all cases.

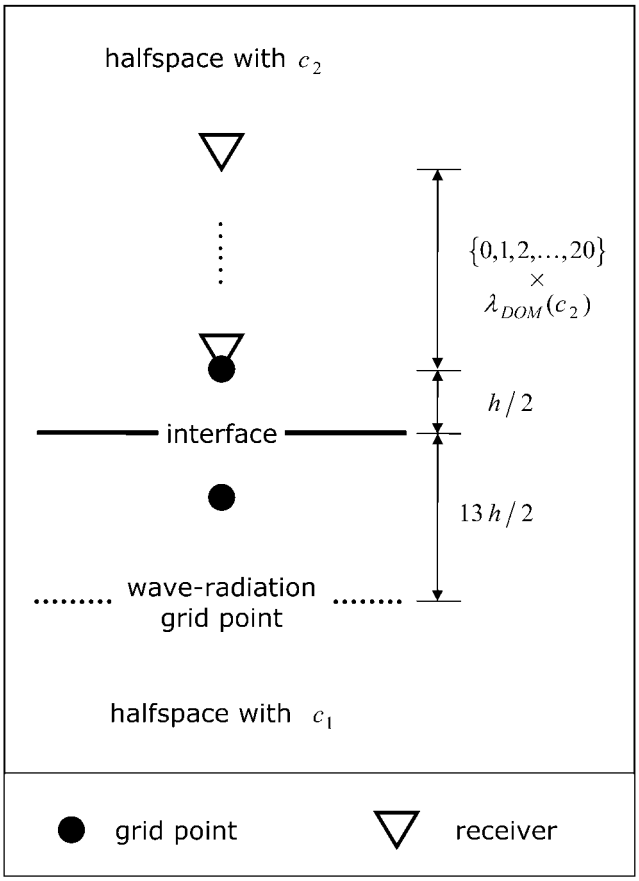

Figure 6. Configuration of a model of two half-spaces. Only grid points for displacement are shown.

Directly at the interface, there is no dramatic difference apparent between Dconv2 and Doptm2 in the considered range of N. This indicates that it is the boundary condition and its numerical approximation that primarily determines the error at the interface.

The error of DSstag4 for $N > 10$ is approximately comparable to the errors of Dconv2 and Doptm2. The envelope misfit of DSstag4 for $N < 10$ is relatively large and, for example, for $N = 5$ is considerably larger than that of Dconv2 and Doptm2 for $N = 10$. At the first sight this might be surprising given the formal 4th-order accuracy of the DSstag4 scheme. In fact, this is not surprising. The use of $N = 5$ in DSstag4 means that the spatial derivative is evaluated over six times larger spatial extent than in the case of $N = 10$ in Dconv2 or Doptm2. Because it is the boundary condition that controls the error at the interface, the larger spatial extent of the DSstag4 operator cannot improve the accuracy at the interface. It is just opposite.

Figure 8 shows results for the same configuration as Figure 7 except the material parameterization: instead of the integral harmonic averaging of elastic moduli, equation (10), the integral arithmetic averaging of elastic moduli is applied. It is obvious that the arithmetic averaging yields considerably larger phase misfits than the harmonic averaging. This is because, as shown theoretically by Moczo *et al.* (2002), the arithmetic averaging is wrong in the 1D case.

Error Away from the Interface

Due to grid dispersion the error of Dconv2 dramatically increases with distance and decreasing N. The increase is steeper for larger c_1/c_2. This is easy to understand. As is well known (e.g., Alford *et al.*, 1974; Marfurt, 1984), grid dispersion of Dconv2 increases with decreasing p. As shown, in the model of two half-spaces p_2 decreases with c_1/c_2.

Note that in the case of the arithmetic averaging of elastic moduli, the error of Dconv2 as a function of distance is not monotonic. This is likely because the arithmetic averaging causes at the interface a time shift with a sign opposite to that caused by grid dispersion in the c_2-half-space.

The increase of the error of Doptm2 is almost negligible.

For a given small N and a given distance the error of DSstag4 is not a monotonic function of c_1/c_2. The error first decreases, then increases with c_1/c_2. The error of DSstag4 in the case of a very small c_1/c_2 dramatically increases with distance even for, for example, $N = 10$. The two latter features can be explained by the dependence of grid dispersion of DSstag4 on p. As already shown, p_2 decreases with c_1/c_2. In the case of the homogeneous unbounded medium, we saw that the error is largest for $p = 1$, decreases down to some minimum and then increases again with decreasing p. A conclusion for DSstag4 is that in a model with a small velocity contrast the error in the slower medium can be very large because of grid dispersion. It can be reduced by using an adjusted, sufficiently small value of the stability ratio, p_1 in our notation, for a chosen N.

Recall Figure 4 that shows curves of minima of the envelope misfit, phase misfit, and sum of the two misfits as functions of N and p, that is, $EM(N, p)$, $PM(N, p)$, and $EM(N, p) + PM(N, p)$. The use of the curves in a homogeneous medium is simple: for a chosen N such p is taken for which $EM(N, p) + PM(N, p)$ takes the minimum value.

In our problem of two half-spaces with $c_1 > c_2$ we are interested in reducing grid dispersion in the half-space with c_2. We can therefore consider such p_2 for which the error takes the minimum value. According to equation (42), p_1 would be

$$p_1 = p_2 \frac{c_1}{c_2}. \tag{43}$$

Because, however, $p_1 < 1$, we can, in fact, consider only such p_2 for which

$$p_2 < \frac{c_2}{c_1}. \tag{44}$$

In our numerical examples shown in Figure 7, $c_2/c_1 \in \{1/1.5, 1/4.1, 1/10.0\} = \{0.67, 0.24, 0.10\}$. This means, that

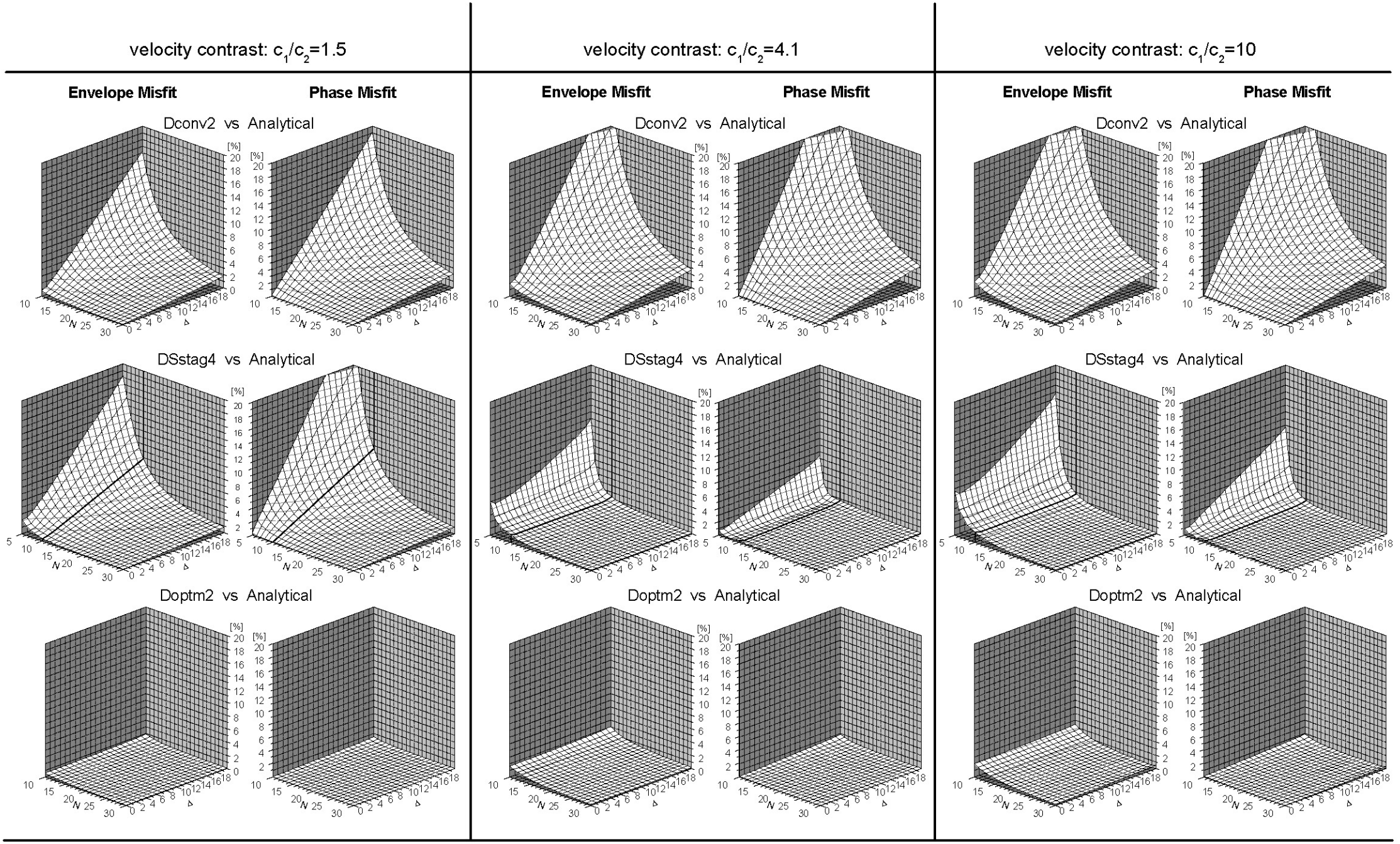

Figure 7. Error due to interface and grid dispersion in a model of two half-spaces: envelope and phase misfits of the FD schemes Dconv2, DSstag4, and Doptm2 as functions of N (the number of grid spacings per λ_{MIN} (c_2)) and Δ (distance in multiples of λ_{DOM} (c_2)). Misfits are shown for three velocity contrasts: $c_1/c_2 \in \{1.5, 4.1, 10.0\}$. The misfits are evaluated relative to the reference analytical solution.

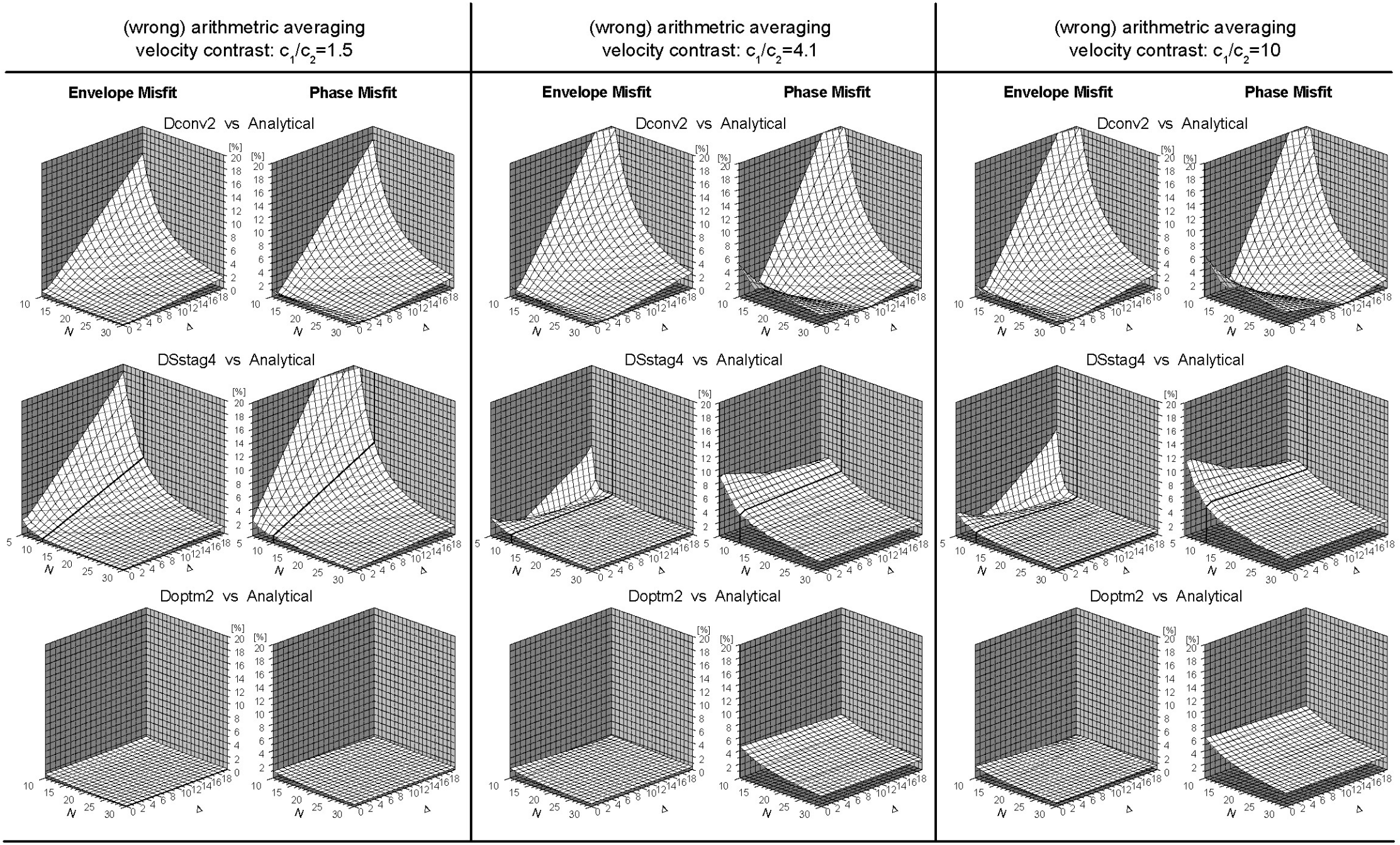

Figure 8. The same as in Figure 5 but with the arithmetic averaging of the elastic moduli. It is clear that the arithmetic averaging yields significantly lower accuracy than the harmonic averaging.

we can adjust values of p_1 for all values of N in the case of $c_2/c_1 = 1/1.5$. In the case of $c_2/c_1 = 1/4.1$ we can only adjust p_1 values for $N \geq 8$. This is because for $N < 8$ the value of p_2 obtained from the minimum curve would yield $p_1 > 1$. Therefore, we take $p_1 = 0.99$. In the case of $c_2/c_1 = 1/10$, due to high-velocity contrast, it is not possible to adjust the value of p_1 for any N.

The modified values of p_1 used for the two cases are shown in the rightmost panel of Figure 9. Misfits of the DSstag4 calculations with adjusted p_1 values are shown in the left and center panels of Figure 9 for $c_1/c_2 = 1.5$ and $c_1/c_2 = 4.1$, respectively. Comparing misfits for $c_1/c_2 = 1.5$ in Figures 7 and 9 we can see that the use of adjusted values of p_1 considerably improved accuracy. On the other hand, there is practically no improvement in the case of $c_1/c_2 = 4.1$ because, due to condition (44), there was no adjustment of p_1 possible for values of N for which the error is large.

Thus, the cases of $c_1/c_2 = 4.1$ and $c_2/c_1 = 1/10$ clearly show that improvement of accuracy in DSstag4 is not always possible by adjusting the p_1 value. The improvement is only possible by using sufficiently large N.

It can be seen from Figures 7 and 9 that at least $N > 10$ should be used in DSstag4 despite the fact that DSstag4 formally is the 4th-order accurate in space. Since the effect of grid dispersion is cumulative, N should increase with the travel distance.

Interior Gradient Layer

Consider an interior layer in a homogenous space with velocity c_1. The upper and lower boundaries of the layer are at z_U and z_L, respectively, and $z_L > z_U$. The velocity inside the layer is given by

$$c(z) = c_1 - \frac{c_1 - c_2}{2}\left\{1 - \cos\left[\frac{2\pi}{H}(z - z_U)\right]\right\}, \quad (45)$$

where $H = z_L - z_U$. The minimum value of $c(z) = c_2$ is in the middle of the layer whereas $c(z) = c_1$ is at the upper and lower boundaries of the layer. The layer thickness H is found from the condition

$$2\int_{z_U}^{z_L} \frac{dz}{c(z)} = \frac{1}{f_{\mathrm{DOM}}}. \quad (46)$$

The obtained thickness is $H = \sqrt{c_1 c_2}/2f_{\mathrm{DOM}}$. N is defined by equation (40). The reference solution for the model of interior gradient layer was calculated by using the analytical solution (27) for a stack of thin homogeneous layers. Figure 10 (left panel) shows convergence of the solution. As a reference solution for evaluation of the misfits of the FD schemes we used the analytical solution with 5000 layers.

In all three schemes the wave is radiated in the half-space with c_1 at distance of six grid spacings from the lower boundary of the layer.

The envelope and phase misfits of the three FD schemes are shown in the middle panel of Figure 10. The errors of Dconv2 and Doptm2 are similar. This is likely because the travel distance inside the layer is small enough to render negligible the error due to grid dispersion which, as was demonstrated, is significantly larger in Dconv2. The error is due more to material heterogeneity than to grid dispersion. The largest errors are in the middle of the layer; this is consistent with the position of the largest amplitude of the fundamental mode excited in the layer. Given the relative complexity of the medium, the two schemes yield plausible results.

The error of DSstag4 is considerably larger than that of the two other schemes. A likely explanation for this is the spatial extent of the 4th-order operator that is relatively large portion of the layer thickness in the case of small N; while that portion is used to approximate the spatial derivative at its central point, the medium changes considerably all the way along that portion.

The right panel of Figure 10 shows the envelope and phase misfits of the schemes with the arithmetic averaging of moduli used instead of the harmonic averaging. It is obvious that the arithmetic averaging yields considerably worse results. The numerical solutions do not converge to the reference solutions in the considered range of N.

Conclusions

We presented a heterogeneous FD scheme, Doptm2, based on the application of the optimally accurate operators developed by Geller and Takeuchi (1998) to the heterogeneous strong formulation of the equation of motion developed by Moczo *et al.* (2002) for the 1D problem. We numerically compared Doptm2 with two other schemes: Dconv2 based on the application of standard conventional 2nd-order FD operators to the heterogeneous strong displacement formulation of the equation of motion for the 1D problem, and DSstag4 based on the application of the staggered-grid 4th-order operators to the heterogeneous strong displacement-stress formulation of the equation of motion for the 1D problem.

The numerical comparisons were performed for three types of models: homogeneous space, two half-spaces in contact, and an interior layer with a strong velocity gradient. The accuracy of the numerical solutions was quantified by evaluating the envelope and phase misfits with respect to the exact analytical solutions.

The main conclusions are summarized as follows.

Grid dispersion in a homogeneous medium:

- The error of Dconv2 (identical with DSstag2) considerably increases with distance because of grid dispersion (except for the theoretical limiting case of p exactly equal to 1,

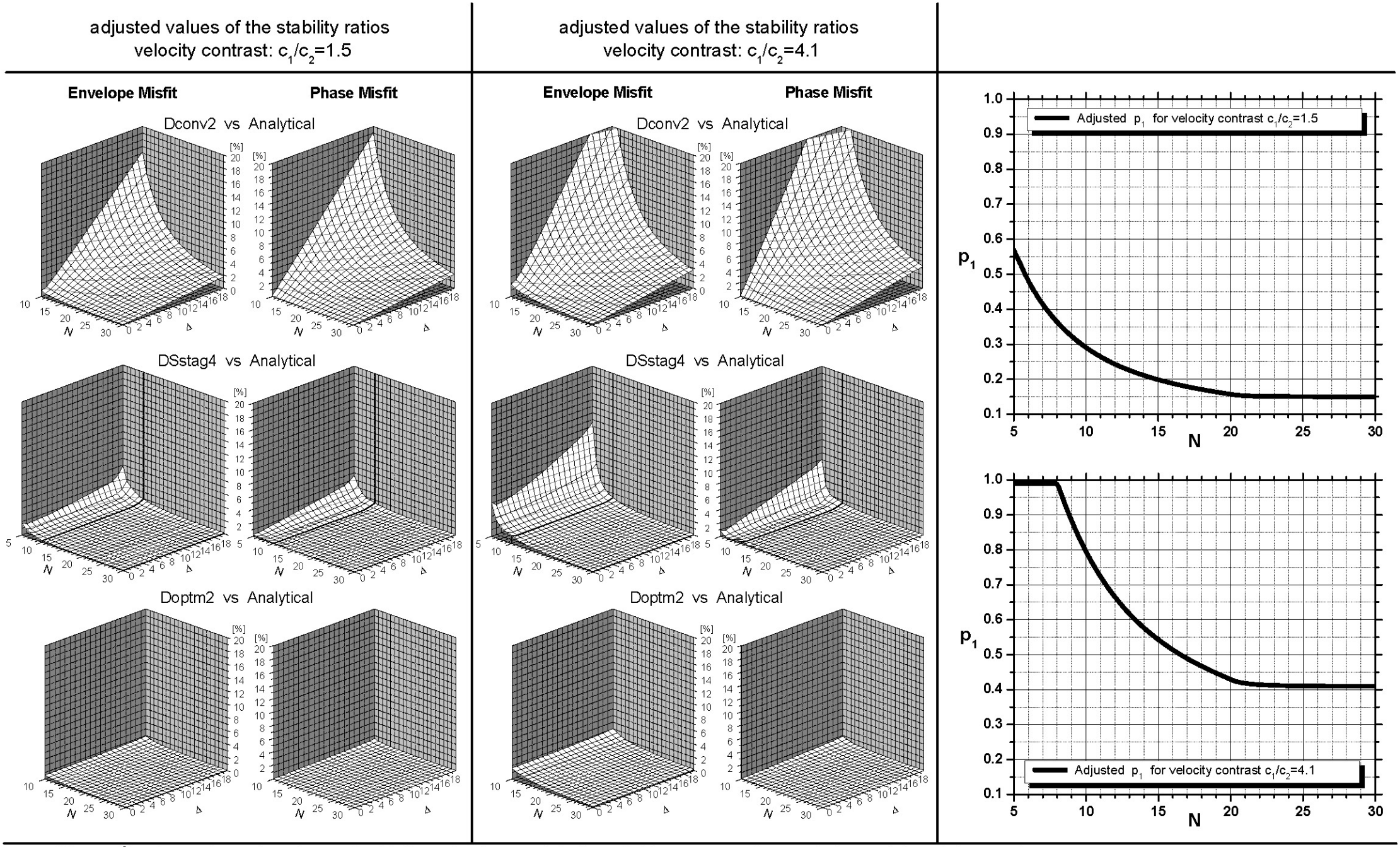

Figure 9. Error due to interface and grid dispersion in a model of two half-spaces: envelope and phase misfits of the FD schemes Dconv2, DSstag4, and Doptm2 as functions of N (the number of grid spacings per $\lambda_{\mathrm{MIN}}\,(c_2)$) and Δ (distance in $\lambda_{\mathrm{DOM}}\,(c_2)$). Misfits are shown for two velocity contrasts: $c_1/c_2 \in \{1.5, 4.1\}$. The misfits are evaluated relative to the reference analytical solution. DSstag4 calculations were performed with the adjusted values of p_1. The errors for Dconv2 and Doptm2 are the same as in Figure 5: they are shown here for convenient comparison with the new results for DSstag4. The rightmost panel shows adjusted values of p_1 used in the calculations by DSstag4.

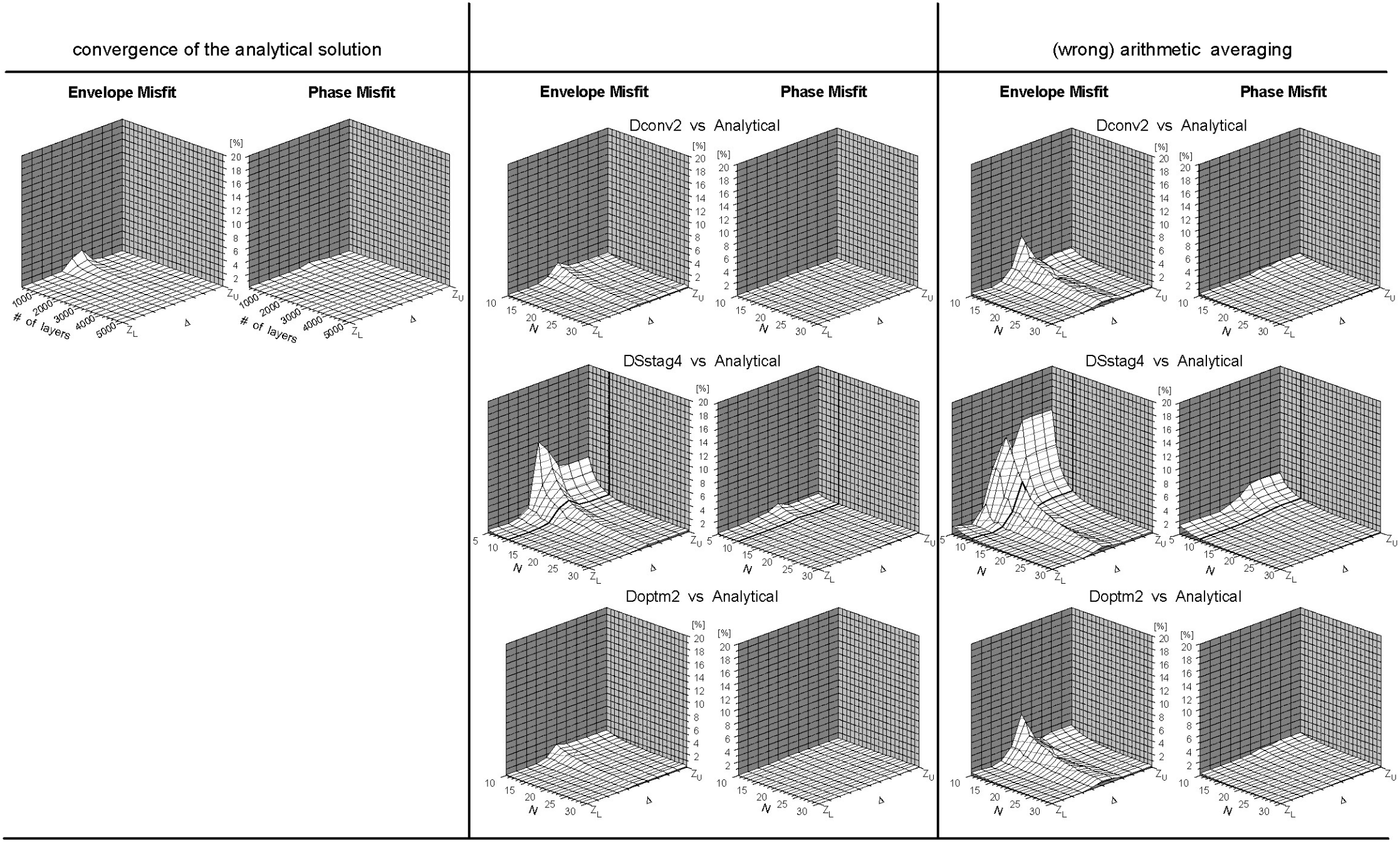

Figure 10. (Left) Convergence of the analytical solution for the increasing number of homogeneous layers used to approximate the smooth velocity gradient. (Center) Error of propagation inside the layer with the velocity gradient: envelope and phase misfits of the FD schemes Dconv2, DSstag4, and Doptm2 as functions of N (the number of grid spacings per λ_{MIN} (c_2)) and position inside the layer; z_L and z_U denote the lower and upper boundaries of the gradient layer. (Right) The same as in the central panel but with the arithmetic averaging of the elastic moduli.

where the scheme is accurate); the error can be reduced by drastic increase of the number of grid spacings per wavelength (N) and using the maximum possible stability ratio (p).
- The error of DSstag4 grows considerably with distance for small N and large p; for a chosen N the error can be reduced by using sufficiently small p that $EM(N, p) + PM(N, p)$ takes the minimum value.
- The error of Doptm2 is negligible compared with those of Dconv2 and DSstag4.
- Despite the formal 4th-order accuracy of DSstag4, for $p = 0.95$ the errors of both DSstag4 and the 2nd-order accurate Dconv2 as functions of N have the same convergence rate, -2, whereas that of Doptm2 is -4.
- While adjustment of the stability ratio p value in DSstag4 is possible in the homogeneous medium (at a price of a small fraction of the maximum possible time step), it is not possible in general in the heterogeneous medium.

Error at the interface:

- The error at the interface is primarily controlled by the boundary condition and its numerical approximation.
- The error weakly grows with the velocity contrast.
- The 4th-order of DSstag4 does not improve the accuracy compared with the 2nd-order schemes.
- The arithmetic averaging of elastic moduli yields significantly lower accuracy than the harmonic averaging.

Error away from the interface:

- For a given N the error of DSstag4 can be reduced by using an adjusted small value of p (and thus small fraction of the maximum possible timestep) only in the case of sufficiently small velocity contrast; in the case of moderate or large velocity contrast the error can be reduced only using sufficiently small spatial grid spacing,
- Despite the formal 4th-order accuracy of DSstag4, the spatial sampling criterion cannot be weaker than that of the formally 2nd-order accurate Doptm2.

Error inside the strong velocity gradient layer:

- The errors of Dconv2 and Doptm2 are comparable, the error of DSstag4 is larger mainly for small N (i.e., larger grid spacings).

The general conclusion is that Doptm2, that is the scheme applying Geller and Takeuchi's (1998) 2nd-order optimally accurate operators to the strong heterogeneous formulation of 1D equation of motion of Moczo *et al.* (2002), is significantly more accurate than the schemes based on the application of the conventional 2nd-order and staggered-grid 4th-order operators.

Acknowledgments

This work was supported by the Marie Curie Research Training Network SPICE Contract no. MRTN-CT-2003-504267. The work was supported in part by the Geophysical Institute, Slovak Academy of Sciences. Discussions with Robert J. Geller, Steven M. Day, and Peter Pazak helped to improve the presentation and are greatly appreciated. The kind arrangement and help of M. Dawid, H. Skvara, and Fallahi during the second author's stay in Vienna are appreciated.

References

Alford, R. M., K. R. Kelly, and D. Boore (1974). Accuracy of finite-difference modeling of the acoustic wave equation, *Geophysics* **39,** 834–842.

Alterman, Z., and F. C. Karal (1968). Propagation of elastic waves in layered media by finite-difference methods, *Bull. Seism. Soc. Am.* **58,** 367–398.

Arntsen, B., A. Nebel, and L. Amundsen (1998). Visco-acoustic finite-difference modeling in the frequency domain, *J. Seism. Explor.* **7,** 45–64.

Boore, D. M. (1970). Love waves in nonuniform waveguides: finite difference calculations, *J. Geophys. Res.* **75,** 1512–1527.

Boore, D. (1972). Finite-difference methods for seismic wave propagation in heterogeneous materials, in *Methods in Computational Physics*, Vol. 11, B. A. Bolt (Editor), Academic Press, New York.

Geller, R. J., and T. Ohminato (1994). Computation of synthetic seismograms and their partial derivatives for heterogeneous media with arbitrary natural boundary conditions using the Direct Solution Method, *Geophys. J. Int.* **116,** 421–446.

Geller, R. J., and N. Takeuchi (1995). A new method for computing highly accurate DSM synthetic seismograms, *Geophys. J. Int.* **123,** 449–470.

Geller, R. J., and N. Takeuchi (1998). Optimally accurate second-order time-domain finite difference scheme for the elastic equation of motion: one-dimensional case, *Geophys. J. Int.* **135,** 48–62.

Holberg, O. (1987). Computational aspects of the choice of operator and sampling interval for numerical differentiation in large-scale simulation of wave phenomena, *Geophys. Prospect.* **35,** 629–655.

Jo, C. H., C. S. Shin, and J. H. Suh (1996). An optimal 9 point, finite difference, frequency-space, 2-D wave extrapolator, *Geophysics* **61,** 529–537.

Kristek, J., P. Moczo, and R. J. Archuleta (2002). Efficient methods to simulate planar free surface in the 3D 4th-order staggered-grid finite-difference schemes, *Stud. Geophys. Geod.* **46,** 355–381.

Kristekova, M., J. Kristek, P. Moczo, and S. M. Day (2006). Misfit criteria for quantitative comparison of seismograms, *Bull. Seism. Soc. Am.* **96,** 1836–1850.

Levander, A. R. (1988). Fourth-order finite-difference P-SV seismograms, *Geophysics* **53,** 1425–1436.

Marfurt, K. J. (1984). Accuracy of finite-difference and finite-element modeling of the scalar and elastic wave equations, *Geophysics* **49,** 533–549.

Mizutani, H. (2002). Accurate and efficient methods for calculating synthetic seismograms when elastic discontinuities do not coincide with the numerical grid, *Ph.D. Thesis*, The University of Tokyo.

Moczo, P., J. Kristek, and L. Halada (2004). *The Finite-Difference Method for Seismologists. An Introduction*, Comenius University, Bratislava. Available in pdf format at ftp://ftp.nuquake.eu/pub/Papers.

Moczo, P., J. Kristek, V. Vavryčuk, R. J. Archuleta, and L. Halada (2002). 3D heterogeneous staggered-grid finite-difference modeling of seismic motion with volume harmonic and arithmetic averaging of elastic moduli and densities, *Bull. Seism. Soc. Am.* **92,** 3042–3066.

Moczo, P., J. O. A. Robertsson, and L. Eisner (2006). The finite-difference time-domain method for modeling of seismic wave propagation, in *Advances in Wave Propagation in Heterogeneous Earth*, R.-S. Wu, V. Maupin, and R. Dmowska (Editors), *Advances in Geophysics*, vol. 48, R. Dmowska (Editor), Elsevier-Pergamon, New York (in press).

Sochacki, J. S., J. H. George, R. E. Ewing, and S. B. Smithson (1991). Interface conditions for acoustic and elastic wave propagation, *Geophysics* **56,** 168–181.

Stekl, I., and R. G. Pratt (1998). Accurate viscoelastic modeling by frequency-domain finite differences using rotated operators, *Geophysics* **63,** 1779–1794.

Strang, G., and G. J. Fix (1973). *An Analysis of the Finite Element Method*, Prentice-Hall, Englewood Cliffs, New Jersey.

Takeuchi, N., and R. J. Geller (2000). Optimally accurate second order time-domain finite difference scheme for computing synthetic seismograms in 2-D and 3-D media, *Phys. Earth Planet. Interiors* **119,** 99–131.

Virieux, J. (1984). SH-wave propagation in heterogeneous media: velocity-stress finite-difference method, *Geophysics* **49,** 1933–1957.

Virieux, J. (1986). P-SV wave propagation in heterogeneous media: velocity-stress finite-difference method, *Geophysics* **51,** 889–901.

Zahradnik, J., P. O'Leary, and J. S. Sochacki (1994). Finite-difference schemes for elastic waves based on the integration approach, *Geophysics* **59,** 928–937.

Faculty of Mathematics, Physics and Informatics
Comenius University
Mlynska dolina F1
842 48 Bratislava
Slovak Republic

Manuscript received 10 February 2006.